Since January 2020 Elsevier has created a COVID-19 resource centre with free information in English and Mandarin on the novel coronavirus COVID-19. The COVID-19 resource centre is hosted on Elsevier Connect, the company's public news and information website.

Talanta Open 6 (2022) 100155

Contents lists available at ScienceDirect

Talanta Open

journal homepage: www.sciencedirect.com/journal/talanta-open

An alternative ready-to-use electrochemical immunosensor for point-of-care COVID-19 diagnosis using graphene screen-printed electrodes coupled with a 3D-printed portable potentiostat

Vitsarut Primpray, Wichayaporn Kamsong, Saithip Pakapongpan, Kanchanok Phochakum, Arissanan Kaewchaem, Assawapong Sappat, Anurat Wisitsoraat, Tanom Lomas, Adisorn Tuantranont, Chanpen Karuwan *

Graphene Sensor Laboratory (GPL), Graphene and Printed Electronics for Dual-Use Applications Research Division (GPERD), National Security and Dual-Use Technology Center (NSD), National Science and Technology Development Agency (NSTDA), Phahonyothin Road Khlong Nueng, Khlong Luang, Pathum Thani 12120, Thailand

ARTICLE INFO

Keywords:
SARS-CoV-2
Poly(pyrrolepropionic acid)
3D-printed detector
Amperometry

ABSTRACT

A severe acute respiratory syndrome coronavirus 2 (SARS-CoV-2) is a cause of worldwide Coronavirus 2019 (COVID-19) disease pandemic. It is thus important to develop ultra-sensitive, rapid and easy-to-use methods for the identification of COVID-19 infected patients. Herein, an alternative electrochemical immunosensor based on poly(pyrrolepropionic acid) (pPPA) modified graphene screen-printed electrode (GSPE) was proposed for rapid COVID-19 detection. The method was based on a competitive enzyme immunoassay process utilizing horseradish peroxidase (HRP)-conjugated SARS-CoV-2 as a reporter binding molecule to compete binding with antibody against the SARS-CoV-2 receptor binding domain (SARS-CoV-2 RBD) protein. This strategy enhanced the current signal via the enzymatic reaction of HRP-conjugated SARS-CoV-2 RBD antibody on the electrode surface. The modification, immobilization, blocking, and detection processes were optimized and evaluated by amperometry. The quantitative analysis of SARS-CoV-2 was conducted based on competitive enzyme immunoassay with amperometric detection using a 3D-printed portable potentiostat for point-of-care COVID-19 diagnosis. The current measurements at -0.2 V yielded a calibration curve with a linear range of 0.01–1500 ng mL^{-1} (r^2 = 0.983), a low detection limit of 2 pg mL^{-1} and a low quantification limit of 10 pg mL^{-1}. In addition, the analyzed results of practical samples using the developed method were successfully verified with ELISA and RT-PCR. Therefore, the proposed portable electrochemical immunosensor is highly sensitive, rapid, and reliable. Thus, it is an alternative ready-to-use sensor for COVID-19 point-of-care diagnosis.

1. Introduction

Coronavirus 2019 (COVID-19) is an infectious disease caused by severe acute respiratory syndrome coronavirus 2 (SARS-CoV-2). World Health Organization (WHO) announced a global pandemic of COVID-19 on March 11, 2020 [1]. Up to early 2022, the numbers of worldwide confirmed COVID-19 cases and deaths are around 400 million and 5.7 million, respectively [2]. Even though COVID-19 vaccines have been invented in order to prevent SARS-CoV-2 infection, the vaccine effectiveness is still limited and the number of new COVID-19 cases continues to rise [2,3]. Thus, the efficient and rapid method for COVID-19 detection is important to identify the infected patients in order to lessen the spread of COVID-19.

Currently, COVID-19 disease can be diagnosed by several methods including nucleic acid test, serological test, and antigen test. Among these, nucleic acid test based on a reverse transcriptase-polymerase chain reaction (RT-PCR) is highly popular since it offers high sensitivity and specificity for quantification of viral RNAs. It can be used for early-stage detection and has been recommended as a gold standard method for COVID-19 diagnosis by WHO and American Center for Disease Control (CDC) [4]. However, the RT-PCR method requires a well-trained operator, multiple steps, long analysis time (~2–4 h), expensive reagents and non-field-deployable instruments [5]. Besides, serological test including enzyme-linked immunosorbent assay (ELISA),

* Corresponding author.
E-mail address: chanpen.kar@nstda.or.th (C. Karuwan).

https://doi.org/10.1016/j.talo.2022.100155
Received 9 August 2022; Received in revised form 30 September 2022; Accepted 2 October 2022
Available online 4 October 2022

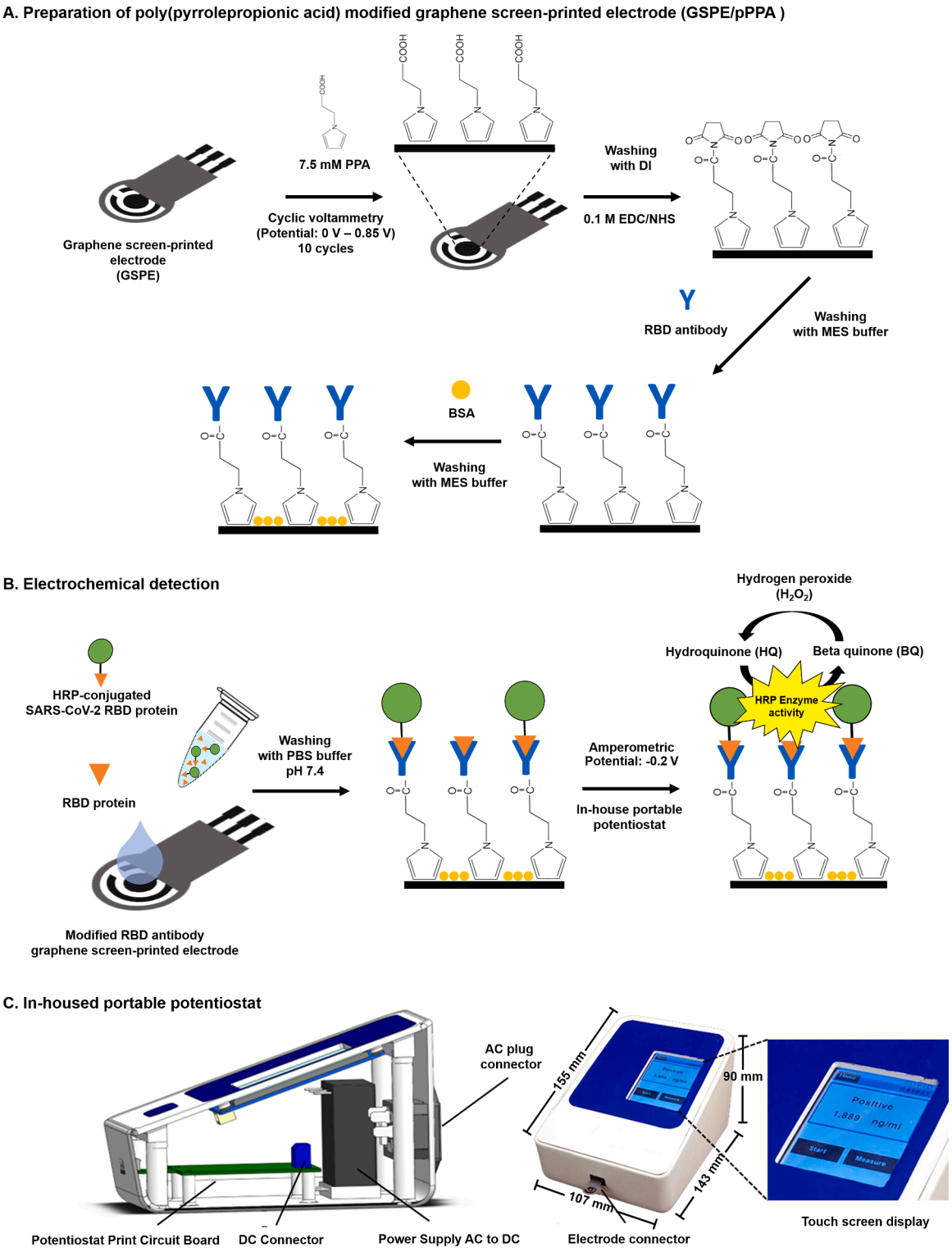

Fig. 1. Schematic illustration of the immunosensor coupled with the in-house portable potentiostat: Preparation of modified graphene screen-printed electrode (A), electrochemical detection process (B) and design of in-house portable potentiostat (C).

chemiluminescence immunoassay (CLIA), and lateral flow immunoassay (LFIA) were used for determining immune response after infection or vaccination for several days [6]. ELISA and CLIA based on enzymatic and luminescent reactions for determination of isotype and titer of antibody are also widely used in laboratories because of high specificity and accuracy. Nevertheless, they are limited by complicated procedures and long analysis times (~ 3–5 h) [5,7]. LFIA is considered as a promising point-of-care test (POCT) method for the identification of isotype antibody owing to ease of use, quick operation and low cost compared with other methods [8]. However, it exhibits limited sensitivity and accuracy [9]. Recently, an antigen test has been increasingly developed from these approaches for early detection of COVID-19 but its sensitivity is still need to be further improved [8–10]. Consequently, alternative electrochemical immunosensors have been proposed to

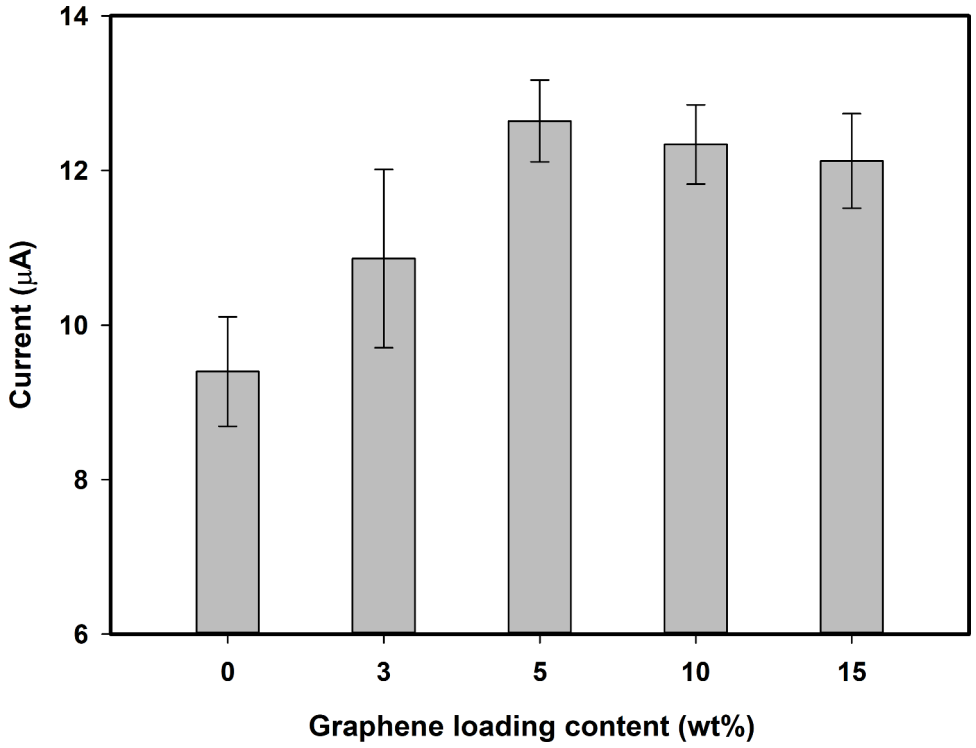

Fig. 2. Effect of graphene loading content on the current response of modified GSPEs to 5 μg mL^{-1} of HRP-conjugated SARS-CoV-2 RBD protein.

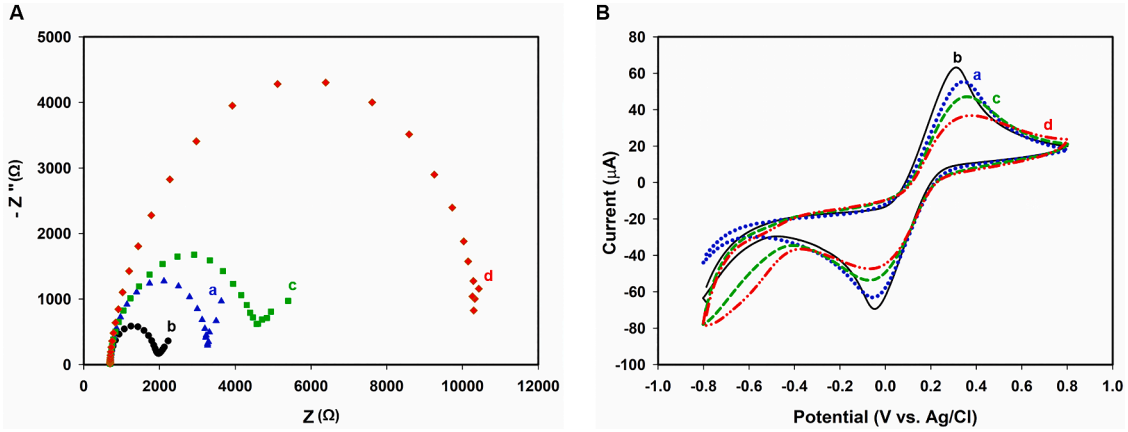

Fig. 3. Nyquist plots (A) and cyclic voltammograms (B) taken with 5 mM $K_3Fe(CN)_6$ in PBS (10 mM, pH 7.4) buffer solution of SPCE (a), GSPE (b), GSPE/pPPA (c) and GSPE/pPPA/RBD ab (d).

overcome the drawbacks of traditional methods. The electrochemical response will be instantly produced from specific interactions between antibodies or other binding molecules such as molecular imprinting polymers (MIP) and targeted antigens on an electrode surface [10–12]. In addition, the electrochemical method is highly sensitive, fast, portable, easy to use and highly attractive for POCT of COVID-19 [13]. Generally, the sensitivity of electrochemical immunosensors for detection of COVID-19 and other biomolecules can be boosted by applying the nanomaterials, particularly graphene and metal nanoparticles, to increase the conductivity and surface area of working electrodes [14–18]. However, these previous methods still provide limited sensitivity and require a professional user to diagnose. The use of appropriate enzymes such as horseradish peroxidase (HRP) can be highly useful to enhance the sensitivity of immunosensors [19,20]. Nevertheless, there are still very few reports of enzymatic electrochemical immunosensors for COVID-19 detection [21].

Herein, an innovative graphene-based enzymatic electrochemical immunosensor coupled with a portable potentiostat was proposed for cost-effective, highly sensitive and selective point-of-care diagnosis of COVID-19. A graphene screen-printed electrode (GSPE) of the immunosensor was fabricated from a mixture of carbon paste and graphene nanoplatelets [22,23]. The GSPE was modified with poly(pyrrolepropionic acid) (pPPA), a suitable conducting polymer for an electrochemical immunosensor [24–26] owing to its high content of carboxyl groups for covalent binding with SARS-CoV-2 receptor-binding domain (RBD) antibody. SARS-CoV-2 was detected via the competitive enzyme immunoassay using the SARS-CoV-2 RBD protein as a competitive compound that could bind to the capturing antibody, leading to a reduced concentration of HRP-conjugated SARS-CoV-2 antigen. Consequently, the electrochemical current signal due to HRP redox would decrease according to the increased concentration of SARS-CoV-2 RBD protein. Moreover, a portable 3D-printed potentiostat was developed to

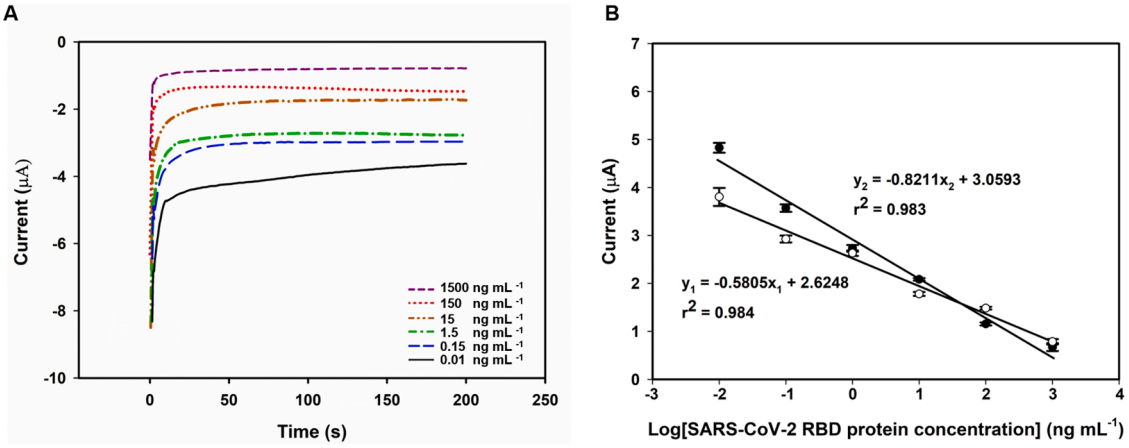

Fig. 4. Amperometric responses of the optimal immunosensor at different concentrations of SARS-CoV-2 RBD protein using the commercial potentiostat (A). Comparison of calibration curves acquired using the commercial potentiostat (○) and in-house portable potentiostat (●) for determination of SARS-CoV-2 RBD protein (B).

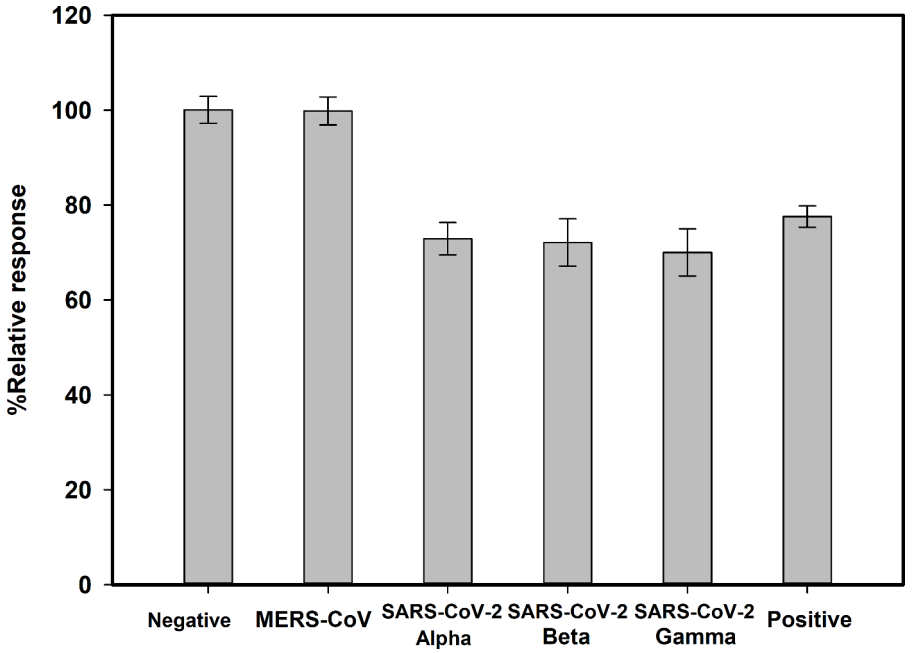

Fig. 5. % Relative response with respect to negative samples of the developed immunosensor for SARS-CoV-2 RBD protein compared against Middle East Respiratory Syndrome Coronavirus (MERS-CoV) as well as Alpha, Beta, and Gamma variations of SARS-CoV-2 at 10 pg mL^{-1}.

Table 1
Comparison of the developed immunosensor and ELISA for the quantification of SARS-CoV-2 RBD protein in nasopharyngeal swab sample ($n = 7$).

Samples	SARS-CoV-2 RBD protein(ng mL^{-1})	Commercial ELISA test kit(ng mL^{-1})	The developed immunosensor(ng mL^{-1})
1	0	0 ± 0	0 ± 0
2	0	0 ± 0	0 ± 0
3	0	0 ± 0	0 ± 0
4	0.1	0 ± 0	0.21 ± 0.10
5	5	5.52 ± 0.01	4.08 ± 1.13
6	10	10.70 ± 0.02	13.66 ± 1.38
7	20	16.23 ± 0.01	17.04 ± 0.85

display positive or negative outcome and convert the current response into the concentration for on-site COVID-19 detection.

2. Material and methods

2.1. Chemical and materials

The commercial inks for screen-printed electrode fabrication comprising carbon paste (CP, Item code: C2030519P4), silver/silver chloride paste (Ag/AgCl, Item code: C61003P7), and insulating paste (Item code: D2070423P5) were purchased from Sun Chemicals (New Jersey, USA). Graphene nanoplatelet powder was acquired from UC Bacon (Taoyuan City, Taiwan). 1H-Pyrrole-1-propionic acid (purity ≥ 97%), MES hydrate (purity ≥ 99%), 1-Ethyl-3-(3-dimethylaminopropyl) carbodiimide hydrochloride or EDC (purity ≥ 99%), N—Hydroxysuccinimide or NHS (purity ≥ 98%), and bovine serum albumin powder or BSA, Hydroquinone (purity ≥ 99%) were ordered from

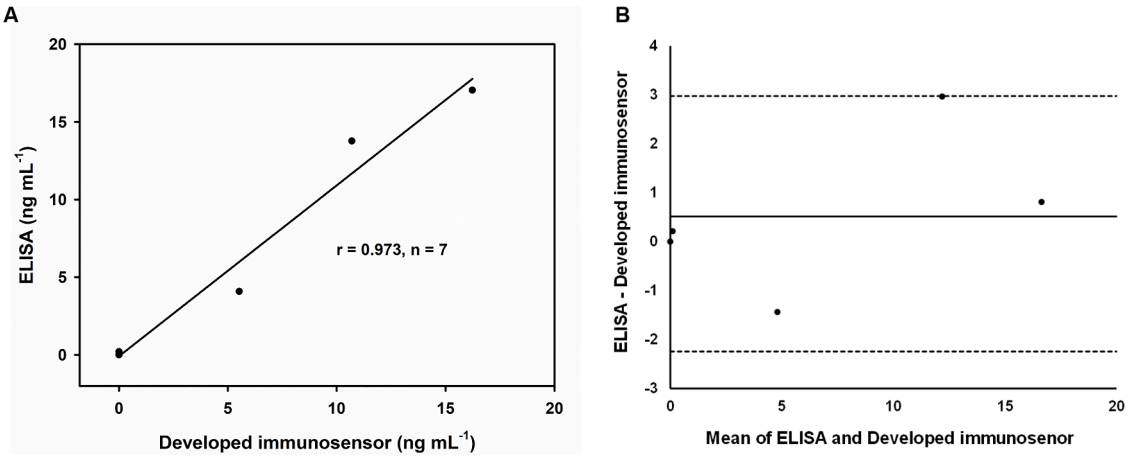

Fig. 6. Scatter correlation plot (A) and Bland-Altman bias plot (B) between the developed immunosensor and ELISA for the quantification of SARS-CoV-2 RBD protein in nasopharyngeal swab samples ($n = 7$).

Table 2
Comparison of the developed immunosensor and RT-PCR for clinical diagnosis of COVID-19 in real nasopharyngeal swab sample ($n = 7$).

Comparison		Rt-PCR		
		+	–	Total
The developed immunosensor	+	3	0	3
	–	0	4	4
	Total	3	4	7

Sigma-Aldrich (St. Louis, MO, USA). 1H-Pyrrole-1-propionic acid was distilled at 75 °C before use. Phosphate buffer saline (PBS, pH 7.2) was bought from Thermo Scientific (Rockford, USA).

SARS-CoV-2 receptor binding domain antibody (cat no.: MBS3014185, purity ≥ 95%), SARS-CoV-2 receptor binding domain protein (cat no.: MBS8574751, purity ≥ 95%), and MERS- CoV Spike S1 recombinant protein (cat no.: MBS434229, purity ≥ 95%) were purchased from MyBioSourcce (San Diego, USA). SARS-CoV-2 Spike Trimer P.1, Gamma variant (cat no.: 100,989–1, purity ≥ 90%) and SARS-CoV-2 Spike Trimer B.1.351, Beta variant (cat no.: 101,091, purity ≥ 90%) were procured from BPS Bioscience (San Diego, USA). SARS-CoV-2 Spike B.1.1.7, Alpha variant (cat no.: 10,748-CV-100, purity ≥ 90%) was obtained from R&D Systems (Minneapolis, Canada). SARS-CoV-2 spike RBD ELISA Kit was ordered from Sino Biological (Beijing, China). HRP Conjugation Kit was acquired from Abcam (Cambridge, UK).

2.2. Instruments

A commercial ball mill machine was used for preparation of graphene ink (Retsch model Emax, Germany). A screen printer was operated to print all screen-printed ink on polyethylene terephthalate (PET) substrates (DEK model 03ix, USA). Cyclic voltammetry (CV) and Electrochemical impedance spectroscopy (EIS) experiments were performed with a commercial potentiostat (AUTOLAB PGSTAT302N, Switzerland).

2.3. Fabrication of the immunosensor

Carbon paste was uniformly mixed with 5 wt% graphene nanoplatelets by ball milling at 1000 rpm for 1 h and then screen-printed onto a PET substrate as graphene screen-printed electrodes (GSPEs) comprising a working electrode (WE) and a counter electrode (CE). The WE was designed to have high active electrode area of 12.57 mm^2 and short electrode length of 25 mm in order to minimize the electrode resistance [27,28]. Next, silver/silver chloride paste was screen printed to form a references electrode (RE) and insulating paste was screen-deposited over parts of electrodes to define active electrode area. GSPE was then modified to attain a COVID-19 immunosensor according to the protocol as displayed in Fig. 1A. GSPE was functionalized with carboxylic group by electro-polymerization via CV between 0.0 to +0.85 V at a scan rate of 100 mV s^{-1} for 10 cycles with 100 μL of pyrrole-1-propionic acid (7.5 mM PPA) prepared in 0.5 M KCl solution [29]. Thereafter, the modified electrodes were rinsed with deionized water and dried at room temperature. The carboxylic acid functionalized electrode was then activated by applying 10 μL of EDC/NHS (0.1 M) in MES buffer (25 mM, pH 5.0), incubating for 30 min at 25 °C and washing with the buffer solution. Finally, the poly (pyrrolepropionic-acid) modified graphene screen-printed electrode (GSPE/pPPA) was obtained and ready for antibody immobilization.

In the immobilization process, 10 μL of SARS-CoV-2 RBD antibody (10 μg mL^{-1}) in MES buffer (25 mM, pH 5.0) was applied to the surface of GSPE/pPPA and incubated for 90 min at 25 °C. Afterward, the immobilized antibody electrode (GSPE/pPPA/RBD ab) was washed with MES buffer (25 mM, pH 5.0). Then, 10 μL of BSA (0.5%, w/v) in MES buffer (25 mM, pH 5.0) was dropped on the working electrode and incubated for 30 min at 25 °C in order to block the unreacted functional groups. Finally, the blocked electrode (GSPE/pPPA/RBD ab/BSA) was washed again with PBS solution (10 mM, pH 7.2) and dried. The electrode was used immediately or stored in a fridge at 4 °C until use.

2.4. Electrochemical characterization

The current response, resistance, and enzymatic response were determined using cyclic voltammetry (CV), amperometry (AMP) and electrochemical impedance spectroscopy (EIS). For CV, the current response to 5 mM $K_3Fe(CN)_6$ in PBS buffer solution (10 mM, pH 7.4) was measured by scanning applied potential between −0.8 V and +0.8 V at scan rate 50 mVs^{-1}. EIS was taken using the same electroltye with an alternating potential amplitude of 0.1 V (vs. Ag/AgCl) over the frequency ranging from 0.01 Hz to 100 kHz. The Nyquist plots of unmodified electrodes and modified electrodes were drawn from the EIS data and corresponding charge transfer resistances (R_{ct}) were calculated. Amperometric measurement was carried out at a fixed applied potential of −0.2 V (vs. Ag/AgCl) for 200 s to evaluate the enzymatic response of HRP-conjugated protein.

2.5. Electrochemical detection

Fig. 1B depicts the proposed detection mechanism on the developed immunosensor. In order to perform the SARS-CoV-2 detection, 10 μL of sample was mixed with 10 μL of HRP-conjugated SARS-CoV-2 receptor

binding domain protein (1 μg mL^{-1}) as an enzymatic reagent in PBS buffer (10 mM, pH 7.4). 10 μL of the mixed solution was then applied to the working electrode, incubated for 90 min at 25 °C and gently washed with PBS buffer (10 mM, pH 7.4) containing 1% BSA. Next, 45 μL of hydroquinone (1 mM) in PBS (50 mM, pH 7.4) as the redox mediator was dropped onto the electrode and a potential of −0.2 V was applied for 100 s to stabilize the electrochemical reaction. After that, 5 μL of hydrogen peroxide (50 mM) in PBS (50 mM, pH 7.4) as the substrate was added onto the electrode and the electrode current was measured at −0.2 V for 200 s (Fig 1B). Finally, the current signal measured at 200 s was used for the calculation of SARS-CoV-2 RBD protein concentration.

2.6. Fabrication of 3D- printed portable potentiostat

An in-house portable potentiostat was designed and manufactured for quantitative analysis of SARS-CoV-2 based on the proposed mechanism using amperometric technique. Its package was assigned as a small medical device (107 mm × 143 mm × 90 mm). It was designed using a solid work program to have a trapezoid shape with a sloped surface on the top to support the display for ease of reading and a front electrode socket for sensor insertion. It was then built by a 3D printing machine (Ender-7 3D Printer) with a polylactic acid plus filament. 3D printing of portable potentiostat was conducted with a nozzle temperature of 190 °C, a base temperature of 65 °C and a printing speed of 250 mm s^{-1}. Polylactic acid plus filament was selected for 3D printing due to low-cost and durability.

The 3D printed device was assembled with a potentiostat printed circuit board (PCB) for measuring the current signal obtained from the detection reaction, a power supply module and a touchscreen display for operating the device through command buttons including Start, Measure and Home buttons (Fig. 1C). The PCB also contained a programmed microcontroller for interpretation of a current response into qualitative and quantitative results within 5 min. In operation, the module would apply a potential of −0.2 V (vs Ag/AgCl) for 100 s after pressing Start button. After that, the message "Add hydrogen peroxide and press Measure button" would be shown on the display. Following the instruction and pushing Measure button, a potential of −0.2 V vs Ag/AgCl would be applied for 200 s while recording the electrochemical signal. The current signal was then converted to the concentration of SARS-CoV-2 RBD protein according to the calibration curve and the result was presented on the display. Finally, home button might be activated for saving energy after finishing the evaluation (see the detail in video as the link in the supplementary information).

2.7. Application to point-of-care diagnosis

To evaluate the practical applicability of the method in COVID-19 point-of-care diagnosis, clinical samples including seven nasopharyngeal swab samples obtained from Ramathibodi Hospital, Bangkok, Thailand were analyzed by our developed immunosensor. The obtained swab samples composed of three positive and four negative samples (clinically confirmed by RT-PCR). Nasopharyngeal swab samples were collected in viral transport mediums without SARS-CoV-2 antigen (n = 7) and spiked with receptor binding domain protein of SARS-CoV-2 at a concentration ranging from 0 to 20 ng mL^{-1}. Each sample was evaluated using our developed immunosensor with the in-house portable potentiostat. The obtained results were compared with a gold standard method for protein detection, namely SARS-CoV-2 Spike protein S1 RBD ELISA Kit, and statistically analyzed using correlation analysis and Bland–Altman plot.

3. Results and discussions

3.1. Optimization of modified GSPE

The functionalization of pPPA on the graphene-based electrode was studied in order to obtain high sensitivity and specificity for SARS-CoV-2 detection. The electropolymerization of pPPA via the CV method with a potential window of 0.0 − 0.85 V at 100 mVs^{-1} was optimized by varying numbers of CV cycles (0 to 25 cycles) and PPA concentrations (0 to 10 mM) in 0.5 M KCl. The result showed that the current signals of bare SPCE had reached a plateau and then decreased after applying more than 5 CV cycles and increasing PPA concentration to more than 5 mM (Fig S1A and S1B). The results could be due to the excessive polymerization of PPA on the electrode surface, disrupting the electron transfer and reducing the conductivity [30–32]. Thus, these conditions were chosen for the functionalization of pPPA on the electrode.

The content of graphene nanoplatelets (GNPs) in GPSE was optimized by varying the GNP amount from 0 to 15 wt% in carbon paste. The electrode was then modified with carboxylic groups of pPPA and immobilized with 50 μg mL^{-1} of SARS-CoV-2 RBD antibody through EDC/NHS coupling chemistry. Finally, the enzymatic current response to 5 μg mL^{-1} of HRP-conjugated SARS-CoV-2 RBD protein was measured as described in Section 2.4. Fig. 2 showed that the HRP enzyme's reaction gradually increased with increasing GNP content from 0 to 5 wt% and remained constant at higher GNP concentrations. This effect might be attributed to the high surface area of graphene, which could improve the immobilization of antibody for binding the enzyme. Thus, 5 wt% GNPs was chosen for the fabrication of GSPEs.

3.2. Characterization of modified GSPE

EIS and CV were used for evaluating charge transfer resistance (R_{ct}) at different steps in the preparation of immunosensor. The R_{ct} values were calculated from Nyquist plots of EIS data as shown in Fig. 3A. The value obtained from GSPE (R_{ct} = 1997 ± 35.46Ω) was lower than that of SPCE (R_{ct} = 3269 ± 42.43 Ω) because graphene nanoplatelet enhanced electron transfer and caused the electrode conductivity to increase, which also led to the increase of current response from 48.18 ± 2.60 μA to 58.15 ± 0.53 μA in the CV results [33]. Moreover, the R_{ct} values of GSPE increased after the modifications with pPPA and SARS-CoV-2 RBD antibody from 1997 ± 35.46 Ω to 4563 ± 69.73 Ω and 10,297 ± 30.96 Ω, respectively. On the other hand, CV results showed that the current responses correspondingly decreased after the modifications (Fig 3B). According to these results, the electron transfer was partially interrupted after modification with pPPA and SARS-CoV-2 RBD antibody due to limited conductivities of the polymer and biomolecules [30,32]. The change in electrode conductivity also confirmed the successful electrode modifications.

3.3. Optimization of process parameters for immunosensor

In order to obtain the highest performance, the processes relating to the immunosensor including immobilization, blocking, and detection were evaluated and optimized via amperometry. Firstly, the immobilization process was the key to enhance the electrode specificity through the specific binding reaction of SARS-CoV-2 RBD antibody. Thus, the antibody concentration and incubation time were varied. Figure S2A and S2B showed that the current response increased with increasing antibody concentration from 0 to 25 μg mL^{-1} before declining as the concentration increased further to 100 μg mL^{-1}. However, there was no significant difference between the current response at 10 and 25 μg mL^{-1}. Therefore, the antibody concentration of 10 μg mL^{-1} was selected as the optimum value. Similarly, the moderate incubation time of 90 min provided the highest current response. The low current responses at high antibody concentrations and long incubation times could be due to the low conductivity of antibody, an insulating biomolecule, which could directly interrupt the electron transfer to and from the working electrode [30,34].

The blocking steps were also optimized to reduce by varying BSA concentrations and blocking times the nonspecific adsorptions of HRP-conjugated SARS-CoV-2 RBD protein by measuring the current

response of a non-immobilized electrode. Figure S3A showed that the electrode without BSA exhibited a higher background current than those with BSA at various BSA concentrations, especially 0.5 w/v%, because the BSA concentration of 0.5 w/v% was sufficient to block the free carboxylic group of pPPA on the electrodes. In addition, the background current obviously decreased with increasing blocking time up to 30 min as demonstrated in Figure S3B. Thus, the optimal condition for the blocking process was 0.5 w/v% BSA and the blocking time of 30 min.

Finally, the electrochemical detection was optimized by varying the concentrations of HRP-conjugated SARS-CoV-2 RBD protein to maximize the competition between SARS-CoV-2 RBD protein as a targeted molecule and HRP-conjugated SARS-CoV-2 RBD protein. In Fig. S4A, the ratio of current signals without and with 100 ng mL^{-1} of SARS-CoV-2 RBD protein (I_0/I_{100}) was maximum at 1.23 for 1 μg mL^{-1} of HRP-conjugated SARS-CoV-2 RBD protein. Moreover, the incubation time was also optimized to obtain the complete binding reaction as presented in Figure S4B. It showed that the current response increased progressively up to the incubation time of 30 min and remained almost the same at longer incubation times. Therefore, these optimal parameters were selected for the immunosensor fabrication and quantitative detection of SARS-CoV-2 RBD protein.

3.4. Analytical performance

The electrochemical current responses of optimally prepared immunosensors were measured under the optimum detection parameters at different concentrations of SARS-CoV-2 RBD protein to construct the calibration curves using the in-house portable potentiostat in comparison with the commercial potentiostat as reported in Fig. 4. It showed that the current signals were decreasing linearly according to the protein concentration in the range of 0.01–1500 ng mL^{-1}. The limit of detection (LOD, 3SD) and limit of quantification (LOQ, 10SD) were calculated using the standard deviation (SD) of the blank signal ($n = 5$) divided by the linear slope of the calibration curves: $y_1 = -0.5862 \times_1 + 2.6286$ ($r^2 = 0.984$, commercial potentiostat) and $y_2 = -0.8113 \times_2 + 3.0092$ ($r^2 = 0.983$, in-house potentiostat). The LODs obtained from commercial and in-house portable potentiostats were 0.9 and 2 pg mL^{-1}, respectively. The LOQ attained from commercial potentiostat was 6 pg mL^{-1} whereas that from in-house potentiostat LOQ was 10 pg mL^{-1}. From the results, LODs and LOQs of both potentiostats were slightly different and lower than those of ELISA assay method for quantification of SARS-CoV-2 RBD protein (LOD = 90 pg mL^{-1}, LOQ = 390 pg mL^{-1}). In addition, the immunosensor exhibited lower LOD than the previous reports based on electrochemical sensors for SARS-CoV-2 RBD protein detection as listed in table S2 [14-17,35-39].

Moreover, the accuracy and precision of the developed immunosensor were evaluated at three different SARS-CoV-2 RBD concentrations (0.15, 15, and 1500 ng mL^{-1}) using five different immunosensors prepared in the same batch. The results were reported in terms of%recovery and relative standard deviation (%RSD) as presented in Table S1. It showed that the%recovery (104%−114%) and%RSD (7.6–12.8) of our developed immunosensors were acceptable in comparison with the standard immunoassay method [40]. Hence, the developed immunosensor was accurate, reliable and suitable for on-site quantitative SARS-CoV-2 RBD protein detection.

3.5. Specificity test

The specificity of the developed immunosensor for SARS-CoV-2 RBD protein was evaluated against Middle East Respiratory Syndrome Coronavirus (MERS-CoV) as well as Alpha, Beta, and Gamma variations of SARS-CoV-2 at 10 pg mL^{-1}. The obtained results were compared with the current signals of the nasopharyngeal swab from normal people as a negative sample in term of%relative response calculated from the percentage ratio of currents from a negative sample to a sample containing each viral antigen as presented in Fig. 5. It demonstrated that the% relative responses of the negative sample and 10 pg mL^{-1} of MERS-CoV were not different, indicating no response and interference from this virus despite its high similarity to SARS-CoV-2. Distinctively, SARS-CoV-2 RBD protein (positive control) and its Alpha, Beta, and Gamma variations provided%relative responses of 77.56 ± 2.26, 72.9 ± 3.4, 72.1 ± 4.9, and 70.03 ± 4.9, respectively. The results indicated that the sensor could effectively differentiate the samples with SARS-CoV-2 RBD protein and its three variations from negative samples because their mean responses were much lower than mean ± 3SD of negative ones (100 ± 6.01). The developed immunosensor could detect SARS-CoV-2 RBD protein and these three variants because they had only three mutations within the receptor-binding domain, which did not affect the binding capacity of immunosensor [41].

3.6. Comparative practical test

The developed immunosensor was practically tested and compared with a commercial ELISA test kit by measuring spiked samples ($n = 7$) as summarized in Table 1. The results of the developed immunosensor and the ELISA test kit agreed well with a high correlation coefficient (r) of 0.973 (Fig 6a). In addition, the Bland–Altman plot displayed that the differences between the measured values from the ELISA test kit and the developed immunosensor lied within ±1.96 SD from the mean value, indicating insignificant statistical difference between the two methods (Fig 6b). In clinical diagnosis, the presence of SARS-CoV-2 in real samples were identified by the developed method and confirmed by RT-PCR as reported in Table 2. The results demonstrated perfect agreement between the two methods, demonstrating that the developed method would be potentially useful for the detection of COVID-19 in real sample.

4. Conclusion

GSPE was successfully developed into an immunosensor for COVID-19 detection based on competitive enzyme immunoassay. The immunosensor was systematically optimized by varying graphene content in GSPE, pPPA modification parameters, antibody immobilization factors and detection conditions. The optimum graphene content of 5 wt% could enhance electron transfer for electrochemical detection. Optimal modification of GSPE with a carboxylic group of pPPA could provide effective covalent immobilization of SARS-CoV-2 RBD antibody. The optimal immunosensor offered high specificity and low SARS-CoV-2 detection limit of 2 pg mL^{-1}. In addition, it could cover three SARS-CoV-2 variants including Alpha, Beta and Gamma. Thus, the developed device was very useful for POCT diagnosis of COVID-19 and might be applicable to other emerging infectious diseases. However, the new variants of concern (VOC) such as Delta (B.1.617.2) and Omicron (B.1.1529 South Africa) currently spreading around the world were not included in this study and should be further investigated in the future.

Declaration of Competing Interest

The authors declare that they have no known competing financial interests or personal relationships that could have appeared to influence the work reported in this paper.

Data availability

The data that has been used is confidential.

Acknowledgment

This work was supported by the National Science and Technology Development Agency [grant numbers P2050842] and the National Research Council of Thailand [grant numbers NRCT: N41A640181]. The

authors would like to thank the Graphene Sensor Laboratory (GPL), Graphene and Printed Electronics for Dual-Use Applications Research Division (GPERD), National Security and Dual-Use Technology Center (NSD), National Science and Technology Development Agency (NSTDA) for provision of research facilities.

Supplementary materials

Supplementary material associated with this article can be found, in the online version, at doi:10.1016/j.talo.2022.100155.

References

[1] D. Cucinotta, M. Vanelli, WHO declares COVID-19 a pandemic, Acta Biomed. Ateneo Parmense 91 (2020) 157–160, https://doi.org/10.23750/abm.v91i1.9397.
[2] WHO, W.H.O. Coronavirus Disease (COVID-19) Dashboard, https://covid19.who.int, 2022 (accessed 4 October 2022).
[3] Pfizer, Pfizer and BioNTech announce vaccine candidate against COVID-19 achieved success in first interim analysis from phase 3 study, https://www.businesswire.com/news/home/20201109005539/en/, 2020 (accessed 4 October 2022).
[4] Centers for Disease Control and Prevention, CDC - 2019-nCoV real-time RT-PCR diagnostic panel, https://stacks.cdc.gov/view/cdc/107932, 2021 (accessed 4 October 2022).
[5] N. Younes, D.W. Al-Sadeq, H. Al-Jighefee, S. Younes, O. Al-Jamal, H.I. Daas, H. M. Yassine, G.K. Nasrallah, Challenges in Laboratory Diagnosis of the Novel Coronavirus SARS-CoV-2, Viruses 12 (2020) 582, https://doi.org/10.3390/v12060582.
[6] S.N. Walker, N. Chokkalingam, E.L. Reuschel, M. Purwar, Z. Xu, E.N. Gary, K. Y. Kim, M. Helble, K. Schultheis, J. Walters, S. Ramos, K. Muthumani, T.R.F. Smith, K.E. Broderick, P. Tebas, A. Patel, D.B. Weiner, D.W. Kulp, SARS-CoV-2 assays to detect functional antibody responses that block ACE2 recognition in vaccinated animals and infected patients, J. Clin. Microbiol. 58 (2020) e01533, https://doi.org/10.1128/JCM.01533-20. -20.
[7] A.P. Espejo, Y. Akgun, A.F. Al Mana, Y. Tjendra, N.C. Millan, C. Gomez-Fernandez, C. Cray, Review of current advances in serologic testing for COVID-19, Am. J. Clin. Pathol. 154 (2020) 293–304, https://doi.org/10.1093/ajcp/aqaa112.
[8] K.M. Koczula, A. Gallotta, Lateral flow assays, Essays Biochem 60 (2016) 111–120, https://doi.org/10.1042/EBC20150012.
[9] A. Santiago, A. Kustov, A.A. Valenzuela, In the shadow of the stars and stripes: testing the malleability of U.S. support for Puerto Rican statehood, J. Elect. Public Opin. Parties (2020) 1–11, https://doi.org/10.1080/17457289.2020.1821037.
[10] R.R.X. Lim, A. Bonanni, The potential of electrochemistry for the detection of coronavirus-induced infections, TrAC Trends Anal. Chem. 133 (2020), 116081, https://doi.org/10.1016/j.trac.2020.116081.
[11] E. Cesewski, B.N. Johnson, Electrochemical biosensors for pathogen detection, Biosens. Bioelectron. 159 (2020), 112214, https://doi.org/10.1016/j.bios.2020.112214.
[12] J. McClements, L. Bar, P. Singla, F. Canfarotta, A. Thomson, J. Czulak, R. E. Johnson, R.D. Crapnell, C.E. Banks, B. Payne, S. Seyedin, P. Losada-Pérez, M. Peeters, Molecularly imprinted polymer nanoparticles enable rapid, reliable, and robust point-of-care thermal detection of SARS-CoV-2, ACS Sensor. 7 (4) (2022) 1122–1131, https://doi.org/10.1021/acssensors.2c00100.
[13] S.S. Mahshid, S.E. Flynn, S. Mahshid, The potential application of electrochemical biosensors in the COVID-19 pandemic: a perspective on the rapid diagnostics of SARS-CoV-2, Biosens. Bioelectron. 176 (2021), 112905, https://doi.org/10.1016/j.bios.2020.112905.
[14] R.M. Torrente-Rodríguez, H. Lukas, J. Tu, J. Min, Y. Yang, C. Xu, H.B. Rossiter, W. Gao, SARS-CoV-2 RapidPlex: a graphene-based multiplexed telemedicine platform for rapid and low-cost COVID-19 diagnosis and monitoring, Matter 3 (2020) 1981–1998, https://doi.org/10.1016/j.matt.2020.09.027.
[15] S. Mahari, A. Roberts, D. Shahdeo, S. Gandhi, eCovSens-ultrasensitive novel in-house built printed circuit board based electrochemical device for rapid detection of nCovid-19 antigen, a spike protein domain 1 of SARS-CoV-2, bioRxiv (2020), https://doi.org/10.1101/2020.04.24.059204.
[16] A. Yakoh, U. Pimpitak, S. Rengpipat, N. Hirankarn, O. Chailapakul, S. Chaiyo, Paper-based electrochemical biosensor for diagnosing COVID-19: detection of SARS-CoV-2 antibodies and antigen, Biosens. Bioelectron. 176 (2021), 112912, https://doi.org/10.1016/j.bios.2020.112912.
[17] B. Mojsoska, S. Larsen, D.A. Olsen, J.S. Madsen, I. Brandslund, F.A. Alatraktchi, Rapid SARS-CoV-2 detection using electrochemical immunosensor, Sensors 21 (2021) 390, https://doi.org/10.3390/s21020390.
[18] R.D. Crapnell, C.E. Banks, Electroanalytical overview: utilising micro- and nano-dimensional sized materials in electrochemical-based biosensing platforms, Microchimica Acta 188 (8) (2021) 268, https://doi.org/10.1007/s00604-021-04913-y.
[19] B. Rezaei, A.M. Shoushtari, M. Rabiee, L. Uzun, W.C. Mak, A.P.F. Turner, An electrochemical immunosensor for cardiac Troponin I using electrospun carboxylated multi-walled carbon nanotube-whiskered nanofibres, Talanta 182 (2018) 178–186, https://doi.org/10.1016/j.talanta.2018.01.046a.
[20] T.A. Freitas, C.A. Proença, T.A. Baldo, E.M. Materón, A. Wong, R.F. Magnani, R. C. Faria, Ultrasensitive immunoassay for detection of Citrus tristeza virus in citrus sample using disposable microfluidic electrochemical device, Talanta 205 (2019), 120110, https://doi.org/10.1016/j.talanta.2019.07.005.
[21] V. Vásquez, M.C. Navas, J.A. Jaimes, J. Orozco, SARS-CoV-2 electrochemical immunosensor based on the spike-ACE2 complex, Anal. Chim. Acta 1205 (2022), 339718, https://doi.org/10.1016/j.aca.2022.339718.
[22] S. Rodsud, W. Limbut, A simple electrochemical sensor based on graphene nanoplatelets modified glassy carbon electrode (GrNPs/GCE) for highly sensitive detection of Yohimbine (YOH), J. Electrochem. Soc. 166 (2019) B771–B779, https://doi.org/10.1149/2.0751910JES.
[23] P. Si, S. Ding, X.-.W. Lou, D.-.H. Kim, An electrochemically formed three-dimensional structure of polypyrrole/graphene nanoplatelets for high-performance supercapacitors, RSC Adv. 1 (2011) 1271–1278, https://doi.org/10.1039/C1RA00519G.
[24] F.R.R. Teles, L.P. Fonseca, Applications of polymers for biomolecule immobilization in electrochemical biosensors, Mater. Sci. Eng. C 28 (2008) 1530–1543, https://doi.org/10.1016/j.msec.2008.04.010.
[25] V. Serafín, L. Agüí, P. Yáñez-Sedeño, J.M. Pingarrón, Electrochemical immunosensor for the determination of insulin-like growth factor-1 using electrodes modified with carbon nanotubes-poly(pyrrole propionic acid) hybrids, Biosens. Bioelectron. 52 (2014) 98–104, https://doi.org/10.1016/j.bios.2013.08.021.
[26] M. Yuqing, C. Jianrong, W. Xiaohua, Using electropolymerized non-conducting polymers to develop enzyme amperometric biosensors, Trends Biotechnol 22 (2004) 227–231, https://doi.org/10.1016/j.tibtech.2004.03.004.
[27] W. Kamsong, V. Primpray, P. Pasakon, C. Sriprachuabwong, S. Pakapongpan, J. P. Mensing, A. Wisitsoraat, A. Tuantranont, C. Karuwan, Highly sensitive and disposable screen-printed ionic liquid/graphene based electrochemical sensors, Electrochem. Commun. 135 (2022), 107209, https://doi.org/10.1016/j.elecom.2022.107209.
[28] M.J. Whittingham, N.J. Hurst, R.D. Crapnell, A. Garcia-Miranda Ferrari, E. Blanco, T.J. Davies, C.E. Banks, Electrochemical improvements can be realized via shortening the length of screen-printed electrochemical platforms, Anal. Chem. 93 (49) (2021) 16481–16488, https://doi.org/10.1021/acs.analchem.1c03601.
[29] D. Beattie, K.H. Wong, C. Williams, L.A. Poole-Warren, T.P. Davis, C. Barner-Kowollik, M.H. Stenzel, Honeycomb-structured porous films from polypyrrole-containing block copolymers prepared via RAFT polymerization as a scaffold for cell growth, Biomacromolecules 7 (4) (2006) 1072–1082, https://doi.org/10.1021/bm050858m.
[30] V. Serafín, R.M. Torrente-Rodríguez, M. Batlle, P. García de Frutos, S. Campuzano, P. Yáñez-Sedeño, J.M. Pingarrón, Electrochemical immunosensor for receptor tyrosine kinase AXL using poly(pyrrolepropionic acid)-modified disposable electrodes, Sens. Actuators B Chem. 240 (2017) 1251–1256, https://doi.org/10.1016/j.snb.2016.09.109.
[31] Y. Gu, J. Wang, M. Pan, S. Li, G. Fang, S. Wang, Label-free impedimetric immunosensor based on one-step co-electrodeposited poly-(pyrrole-co-pyrrole-1-propionic acid) and reduced graphene oxide polymer modified layer for the determination of melamine, Sens. Actuators B Chem. 283 (2019) 571–578, https://doi.org/10.1016/j.snb.2018.12.046.
[32] H. Dong, C.M. Li, W. Chen, Q. Zhou, Z.X. Zeng, J.H.T. Luong, Sensitive amperometric immunosensing using polypyrrolepropylic acid films for biomolecule immobilization, Anal. Chem. 78 (2006) 7424–7431, https://doi.org/10.1021/ac060657o.
[33] H. Wu, Q. Lin, C. Batchelor-McAuley, R.G. Compton, Nanoimpacts reveal the electron-transfer kinetics of the ferrocene/ferrocenium couple immobilised on graphene nanoplatelets, ChemElectroChem 3 (2016) 1478–1483, https://doi.org/10.1002/celc.201600296.
[34] M. Moreno-Guzmán, I. Ojeda, R. Villalonga, A. González-Cortés, P. Yáñez-Sedeño, J.M. Pingarrón, Ultrasensitive detection of adrenocorticotropin hormone (ACTH) using disposable phenylboronic-modified electrochemical immunosensors, Biosens. Bioelectron. 35 (2012) 82–86, https://doi.org/10.1016/j.bios.2012.02.015.
[35] B.S. Vadlamani, T. Uppal, S.C. Verma, M. Misra, Functionalized TiO2 nanotube-based electrochemical biosensor for rapid detection of SARS-CoV-2, Sensors 20 (2020) 5871, https://doi.org/10.3390/s20205871.
[36] M.A. Ali, C. Hu, S. Jahan, B. Yuan, M.S. Saleh, E. Ju, S.-.J. Gao, R. Panat, Sensing of COVID-19 antibodies in seconds via aerosol jet nanoprinted reduced-graphene-oxide-coated 3D electrodes, Adv. Mater. 33 (2021), 2006647, https://doi.org/10.1002/adma.202006647.
[37] M.Z. Rashed, J.A. Kopechek, M.C. Priddy, K.T. Hamorsky, K.E. Palmer, N. Mittal, J. Valdez, J. Flynn, S.J. Williams, Rapid detection of SARS-CoV-2 antibodies using electrochemical impedance-based detector, Biosens. Bioelectron. 171 (2021), 112709, https://doi.org/10.1016/j.bios.2020.112709.
[38] A. Ahmadivand, B. Gerislioglu, Z. Ramezani, A. Kaushik, P. Manickam, S. A. Ghoreishi, Functionalized terahertz plasmonic metasensors: femtomolar-level detection of SARS-CoV-2 spike proteins, Biosens. Bioelectron. 177 (2021), 112971, https://doi.org/10.1016/j.bios.2021.112971.
[39] A. Raziq, A. Kidakova, R. Boroznjak, J. Reut, A. Öpik, V. Syritski, Development of a portable MIP-based electrochemical sensor for detection of SARS-CoV-2 antigen,

Biosens. Bioelectron. 178 (2021), 113029, https://doi.org/10.1016/j.bios.2021.113029.

[40] U. Andreasson, A. Perret-Liaudet, L.J.C. van Waalwijk van Doorn, K. Blennow, D. Chiasserini, S. Engelborghs, T. Fladby, S. Genc, N. Kruse, H.B. Kuiperij, L. Kulic, P. Lewczuk, B. Mollenhauer, B. Mroczko, L. Parnetti, E. Vanmechelen, M. M. Verbeek, B. Winblad, H. Zetterberg, M. Koel-Simmelink, C.E. Teunissen, A practical guide to immunoassay method validation, Front. Neurol. 6 (2015) 179, https://doi.org/10.3389/fneur.2015.00179.

[41] A. Aleem, A.B. Akbar Samad, A.K. Slenker, Emerging variants of SARS-CoV-2 and novel therapeutics against Coronavirus (COVID-19), StatPearls (2022). https://www.ncbi.nlm.nih.gov/books/NBK570580/.